Achieving Ultrahigh Power Factor In *n*-type Ag_2Se Thin Films By Carrier Engineering

Zhuang-hao ZHENG
Shenzhen University
Jun-yu NIU
Shenzhen University
Tian-bao CHEN
Shenzhen University
Yuexing Chen (chenyx@szu.edu.cn)
Shenzhen University
Fu LI
Shenzhen University
Jing-ting LUO
Shenzhen University
Guang-xing LIANG
Shenzhen University
Shuo CHEN
Shenzhen University
Hong-li MA
Sciences Chimiques de Rennes: Institut des Sciences Chimiques de Rennes
Xiang-hua ZHANG
Sciences Chimiques de Rennes: Institut des Sciences Chimiques de Rennes
Ping FAN
Shenzhen University

Research Article

Keywords: Ag2Se, Thin film, Co-evaporation, Power factor

Posted Date: August 25th, 2021

DOI: https://doi.org/10.21203/rs.3.rs-827728/v1

Version of Record: A version of this preprint was published at Materials Today Energy on December 1st, 2021. See the published version at https://doi.org/10.1016/j.mtener.2021.100933.

Abstract

Ag_2Se is a promising *n*-type material which has been proposed for thermoelectric (TE) application. Achieving high TE power factor for Ag_2Se thin film to use in micro and wearable electronic systems has recently attracted great attention. In present work, Ag_2Se thin films were prepared via a simple co-evaporation method, which provides an effective way for adjusting its composition. By selective modification of Ag content, the carrier concentration is optimized, leading to a *PF* of 6.27 $\mu Wcm^{-1}K^{-2}$. Furthermore, the carrier mobility increased while carrier concentration is maintained after performing an annealing process, thus contributes to relatively high Seebeck coefficient and decent electrical conductivity for $Ag_{2.05}Se$ film annealed at 423 K. As a result, a record-high power factor of 20.51 $\mu Wcm^{-1}K^{-2}$ at 393 K is achieved, which is the best result of the Ag_2Se thin film prepared by evaporation method. This work has opened the way for environmentally friendly room-temperature thermoelectricity.

Introduction

Thermoelectric (TE) materials can utilize Seebeck effect to generate energy from the conversion between heat and electricity [1–5]. TE devices fabricated based on TE materials have wide applications in daily life, aerospace, military and other fields due to the advantages of long service life, and non-polluting [6–10]. The performance of TE material is determined by the dimensionless figure of merit *ZT* ($ZT = S^2\sigma T/\kappa$), which defined by conductivity σ, Seebeck coefficient *S*, thermal conductivity κ and absolute temperature T, respectively [11–14]. For low dimensional TE materials, especially thin films, power factor ($PF = S^2\sigma$) is more usually used to characterize their TE performance.

Due to potential applications in miniature and wearable devices, achieving high performance TE thin film is highly desired. Despite high *ZT* value thin films fabricated based on traditional Te-based materials have been reported, non-environmentally friendly and poor mechanical property still limits their application [15]. Silver selenide (Ag_2Se) is a promising *n*-type TE material and a high *ZT* of 0.96 at 390 K with excellent mechanical property was investigated by X. Shi [16]. Therefore, various methods in recent years have been employed to fabricated Ag_2Se thin films in order to achieve high TE performance and mechanical properties thin film to meet the demand of device manufacturing [17–22]. For instance, Ding et al. have produced this flexible substance on the Nylon layer by hot-pressed. The power factor of their exploration is 9.87 $\mu Wcm^{-1}K^{-2}$ at room temperature [21]. Zhou et al. synthesized the Ag_2Se thermoelectric thin films by using pulsed laser deposition method and achieved high *PF* about 17.5 $\mu Wcm^{-1}K^{-2}$ at room temperature [20]. Gao et al. achieved high *PF* of 24.51 $\mu Wcm^{-1}K^{-2}$ by hydrothermal method of paper-supported Ag_2Se film [22].

Since both Ag and Se are easy oxidized, it can be expected that the vacuum physical vapor deposition technique should be more suitable for the preparation of Ag_2Se thin film materials [23–26]. Definitely, Gonzalez et al. obtained a record power factor of 24.4 $\mu Wcm^{-1}K^{-2}$ in stoichiometric Ag_2Se film grown by pulsed hybrid reactive magnetron sputtering, which is comparable with that of the state-of-the-art bulk

Ag_2Se [17]. Thermal evaporation method is one of the most commonly used vacuum physical vapor deposition techniques that have been reported for preparing excellent TE performance thin films, such as Bi_2Te_3, Cu_2Se and Sb_2Se_3 [27–29]. However, Ag_2Se thin films prepared by this method has low power factor [30–32]. Optimization of the carrier concentration and mobility can effectively improve the thermoelectric performance of TE thin films to some extent [33]. To further enhance the TE performance of evaporated Ag_2Se thin films, it is imperative to integrate multiple approaches to tune the highly interconnected thermoelectric properties [34–36]. In this work, Ag_2Se thin films were prepared by a facile thermal co-evaporation method, instead of using single evaporated, which provides an effective way to adjust composition. The selective modification of Ag content can markedly increase the carrier concentration and enhance the electrical conductivity. Moreover, further annealing can effectively decrease the micro-structure defects of the films, leading to the enhancement of Seebeck coefficient. Accordingly, the power factor of 20.51 $\mu Wcm^{-1}K^{-2}$ is achieved at 393 K, which is a record value of the Ag_2Se thin films prepared by evaporation methods.

Experiment

Ag_2Se based thin films were deposited at room temperature by thermal co-evaporation method. High purity Ag powder (99.99 %) and Se powder (99.99 %) were fixed in a vacuum deposition chamber by using tantalum evaporator boats. The BK7 glass was used as substrates with a dimension of 20 mm × 20 mm × 2 mm and ultrasonic cleaned for 10 minutes sequentially in acetone, ethanol, and deionized water. The background pressure was maintained at 6.5×10^{-4} Pa. The working current of silver source is 160 A, and selenium source stabilized at 40 A with the deposition time was both 15 min. All the Ag powder and Se powder were evaporated after deposition process. The weight ratio of Ag powder and Se powder was reasonably regulated in order to control the composition of Ag and Se in the thin films. Annealing process was further employed in the glove compartment after the optimal composition ratio was confirmed.

X-ray diffraction (XRD, D/max 2500 Rigaku Corporation, CuK_α radiation with the angle of 20° – 60° under 0.02° per step) was applied to analyze the crystal orientation. The surface morphology and element distribution were characterized by a scanning electron microscope (SEM, Zeiss supra55), transmission electron microscopy (TEM, Titan Cubed Themis G201, FEI) with an energy dispersive spectrometer (EDS, Bruker EDS QUANTAX). The electrical conductivity and Seebeck coefficient were measured by utilizing a Seebeck coefficient and electrical conductivity apparatus (SBA458, Nezsch). Van der Pauw Hall measuring instrument (HL5500 PC, Nanometrics) was applied to investigate the carrier concentration and mobility. X-ray photoelectron spectroscopy (XPS, Thermo escalab 250Xi Thermo Fisher) provided semi-quantitative information of the elemental valence states. Variable temperature XRD (SmartLab 3KW Rigaku Corporation) reacts the fact that the sample undergoes a phase transition at 406 K. The bandgap was determined from the reflection spectra obtained on UV-VIS-NIR spectrometer (UV-3600Plus Shimadzu Corporation).

Results And Discussion

Table 1 shows the composition content of Ag_2Se thin films measured by EDS and it can be seen that the actual atomic ratio is close to the nominal atomic ratio of the powder. In order to better recognize, the films were named by using nominal atomic ratio as $Ag_{1.65}Se$, $Ag_{1.75}Se$, $Ag_{1.85}Se$, $Ag_{1.95}Se$, $Ag_{2.05}Se$, $Ag_{2.15}Se$ and $Ag_{2.25}Se$, respectively.

Table 1
Nominal atomic ratio of Ag and Se powder before evaporate and the actual content of the thin films measured by EDS

Nominal atomic ratio (Ag : Se)	**1.65**	**1.75**	**1.85**	**1.95**	**2.05**	**2.15**	**2.25**
Ag(at%)	61.5	62.2	65.6	66.3	67.3	68.3	70.0
Se(at%)	38.5	37.8	34.4	33.7	32.7	31.8	30.0
Actual atomic ratio (Ag : Se)	1.6	1.65	1.91	1.97	2.06	2.15	2.33

Figure 1(a) shows the X-ray diffraction patterns of thin films, and indicates three main peaks located at ~ 33.5°, ~ 34.7° and ~ 36.9° for all the patterns, corresponding to the (112), (121) and (013) planes of Ag_2Se polycrystalline (PDF#24-1041) [37]. The $Ag_{1.65}Se$ and $Ag_{1.75}Se$ samples contain a weak impurity peak at ~ 29.5°, belonging to Se phase (PDF#06-0362), and it disappears after further increased Ag content. Meanwhile, all the samples have Ag impurity peak at ~ 38.1° and the peak (PDF#04-0783) intensity increase with increase of Ag content as shown from the illustrate inset in the right side of Fig. 1(a). The elemental mappings as shown in Fig. 2(b) confirm some Se clusters in the Se-rich sample [38], and no Se-rich when Ag increases, which matched the XRD result. However, some big particles are observed in the surface of Ag-rich thin film and confirms as Ag clusters [30], indicating that there are some component defects in the thin film deposited at room temperature, which are mainly due to insufficient atomic energy as shown from the surface morphology in Fig. S1 (Supporting information).

Figure 2(a) shows the room-temperature electrical conductivity σ, Seebeck coefficient S, and power factor PF of the Ag_2Se based thin films. The σ increases with the rising of Ag content, while the S has a negative change trend. As a comprehensive result, PF firstly increases, reach a maximum value of 6.27 $\mu Wcm^{-1}K^{-2}$, and then decreases. According to the Mott equation [1], both the σ and S is determined by carrier concentration n and mobility μ:

$$\sigma = en\mu \quad (1)$$

$$S = \frac{8\pi^2 k_B^2 T m^*}{3eh^2}\left(\frac{\pi}{3n}\right)^{2/3} \quad (2)$$

m^* is the effective mass of electrons. Thus, the Hall measurement is analyzed and Fig. 2(b) displays the n and μ as function of Ag to Se atomic ratio. The n of the $Ag_{1.55}Se$ is 3.3×10^{18} cm^{-3}, and greatly increases to over 14.0×10^{18} cm^{-3} after the atomic ratio raised over 2.05, while μ decreases from to 650 $cm^{-2}V^{-1}s^{-1}$ to 400 $cm^{-2}V^{-1}s^{-1}$. Comparatively, the change of carrier concentration is more distinct than

the mobility due to disappeared Se defect and increase of Ag content, thus attributing to the greatly enhancement of σ [33, 34, 39].

Although thin films deposited at room-temperature have high carrier concentration, some Ag clusters component defects observed from the SEM results, resulting low μ mobility, and thus cause the low power factor [33]. Annealing has been reported as an efficient way that can reduce the component defects and increase the grain size of the thin films, leading to high mobility which benefits to achieve high TE performance [22]. Thus, $Ag_{2.05}Se$ sample with maximum *PF* value was annealed and the temperature was set as 375 K, 393 K, 403 K, 413 K, 423 K, 453 K, 483 K, 513 K and 543 K, respectively. Figure 3(a) shows the σ, *S*, and *PF* as function of annealing temperature. It indicates that both σ and *S* are increased after annealing, and all the annealed thin films have higher σ and *S* values than that of the as-deposited sample. A maximum value of 17.62 $\mu Wcm^{-1}K^{-2}$ is obtained from the sample annealed at 423 K, which is over 200 % enhancement compare with the as-deposited sample. Figure 3(b) shows the *n* and μ as a function of annealing temperature. The *n* firstly increases and then decreases with the increasing annealing temperature, which is well matched with the change of σ. EDS measurement of $Ag_{2.05}Se$ films annealed at different temperature as shown in the Table S1 indicates the Se content slightly decreased after annealing, resulting in the decreased of *n.* Especially, carrier mobility has greatly increased from of 400 $cm^{-2}V^{-1}s^{-1}$ as-deposited sample to over 600 $cm^{-2}V^{-1}s^{-1}$ with the slightly affect in the carrier concentration when the annealing temperature was over 393 K, benefiting to achieve high *S* and results in relatively high *PF*. Additionally, temperature dependence TE performance of sample annealed at 423 K is shown in Fig. 3(c) and indicates an increasing trend with the increasing test temperature. The σ of 1526.5 Scm^{-1}, *S* of 115.9 μVK^{-1} are obtained at 393 K, contributing to a maximum *PF* of 20.51 $\mu Wcm^{-1}K^{-2}$. The achieved *PF* values at room temperature and 393 K are the record high values of the Ag_2Se thin films prepared by thermal evaporation method as shown in Fig. 3(d).

Figure 4(a) shows the X-ray diffraction patterns of the annealed thin films. All the thin films show the primary Ag_2Se phase with a weak impurity Ag phase related peak. With the increase of annealing temperature, the intensity of (112) peak increases and (121) peak decrease, which is more closed to the typical α-phase Ag_2Se. The binding states of Ag and Se elements in the $Ag_{2.05}Se$ thin film are investigated by XPS and the results are illustrated in Fig. 4(b) and 4(c). As shown in Fig. 4(b), the core level spectrums reveal that the sample have two strong peaks located at ~ 368.4 eV of Ag $3d_{5/2}$ and ~ 374.2 eV of Ag $3d_{3/2}$, which agree with the spin-orbit phenomena of Ag and Ag^+, respectively [40]. A broad peak ranging from 52 to 56 eV is observed and can be identified into two symmetric peaks to be assigned to Se $3d_{5/2}$ and Se $3d_{3/2}$ located at ~ 54.2 and ~ 54.9 eV, which is the characteristic shape of Se(−Ⅱ) in a consistent bonding environment as shown in Fig. 4(c) [40]. Thus, these analyses indicate that the chemical states of the elements of the thin films are Ag^+ and Se^{2-}, respectively. SEM images of the samples are shown in Fig. S2 and indicates that the surface of all the thin films have Ag clusters. However, more Ag spherical-liked clusters is observed when the annealing temperature was over 483 K. These independence Ag clusters in the thin film surface (Fig. S3) will act as a combining center, thus

causes the decrease of electrical conductivity [30]. The content of Se is slightly decreased after annealing, as shown in EDS results (Table S1), suggesting that the aggravation of element diffusion during the annealing process led to the strength of Ag clusters and the loss of Se. Similar phenomenon is also reported by Jindal *et al*. [30, 32].

It is worth noting that the annealing temperature corresponding to the sharp increase in the carrier mobility is near the phase-transition temperature from α-phase to β-phase of Ag_2Se (In-situ XRD is shown in Fig. S4). Thus, in order to further investigate the factor, the unannealed $Ag_{2.05}Se$ sample and annealed sample at 423 K have been analyzed by TEM. As shown in Fig. 5 (a), screw dislocations with length of ~ 100nm are observed for unannealed thin film. Moreover, Ag vacancies in the lattice are observed in Fig. 5(a), which are furthered confirmed by the intensity line profile of the square root of STEM intensity. It can be speculated that there is still a lack of Ag in some regions due to the Ag-clusters, despite the thin film is slight Ag-rich. As mentioned above in SEM analysis (Fig. 1) that some independent Ag clusters distributes in the thin film's surface due to the limit of diffusion energy of the atoms when the thin film deposited at room temperature. For annealed $Ag_{2.05}Se$ film, no dislocation defects are observed in the measurement region and Ag vacancy also disappeared from the grains, indicating the redistribution of atoms during the annealing process. The reduction of defects is beneficial to transport of carriers, and the vanishment of Ag vacanicies leads to the decrease of electron concentration. The results consist with the transport properties as displayed in Fig. 3. Meanwhile, the calculation in Fig. 5(c) and Fig. 5(d) shows that the Ag_2Se with Ag vacancy has smaller bandgap than that of the complete Ag_2Se. We have established a cell with a volume of 2×2×1. And the K point we selected is 3×3×3. We followed the geometrical optimization method BFGS which the convergence standard is the energy of a single atom of 1.0×10^{-5} eV, the interaction force between atoms of 0.03 $eVnm^{-1}$, the stress in the crystal of 0.05 GPa, and the maximum displacement of atoms of 0.0001 nm. We used Generalized Gradient Approximation (GGA) in the form of Perdew-Burke-Ernzerhof (PBE) to describe the exchange correlation energy:

$$E_{xc}^{GGA}[\rho] = \int f_{xc}\left(\rho(\boldsymbol{r}), |\nabla\rho(\boldsymbol{r})|\right)d\boldsymbol{r}$$

and used the ultra-soft pseudopotential to express the interaction between electrons and ions [34]. The electron wave function generated by plane waves with truncate energy of 300 eV. In Fig. S5, the measured optical bandgap confirms that the films have larger optical bandgap after annealing, which match the calculated result. Additionally, more Ag atoms can enter into the β-phase lattice than the α-phase as reported in the literatures [35, 36]. Therefore, it can be inferred that the intensified atomic diffusion at the annealing temperature over phase change temperature will reduce dislocation defects and Ag vacancy defects in the Ag_2Se thin film, thus contributes in the enhancement of carrier mobility and results in relative high *S*.

Conclusion

In summary, we fabricated Ag_2Se based thin film at room temperature by using a facile thermal co-evaporation method. High electrical conductivity of Ag_2Se thin films is achieved after carrier concentration optimization by controlling Ag content, resulting in a maximum power factor of 6.27 $\mu Wcm^{-1}K^{-2}$. Subsequently, the *S* of the prepared thin films are enhanced via annealing according to the relative high carrier mobility due to the reduced dislocation defects and Ag vacancy defects after annealing. As a result, an ultrahigh *PF* of 17.62 $\mu Wcm^{-1}K^{2}$ at room temperature and 20.51 $\mu Wcm^{-1}K^{2}$ at 393 K has been obtained. The overall performance of TE properties studied in this work is comparable or even higher than that of previously reported Ag_2Se thin films prepared by thermal evaporation method.

Declarations

Acknowledgments

This work was supported by the National Natural Science Foundation of China (Grant No. 11604212), Guangdong Basic and Applied Basic Research Foundation (2020A1515010515 and 2019A1515110107), and Science and Technology plan project of Shenzhen (20200811230408001). The authors are thankful for the assistance on STEM-HAADF observation received from the Electron Microscope Center of the Shenzhen University.

References

1. Fan P, Huang XL, Chen TB et al. α-Cu2Se thermoelectric thin films prepared by copper sputtering into selenium precursor layers. *Chemical Engineering Journal* 2021
2. Liu ZY, Zhu JL, Tong X et al (2020) A review of CoSb3-based skutterudite thermoelectric materials: A review. Journal of Advanced Ceramics 9(6):647–673
3. Xu W, Zhang ZW, Liu CY et al (2021) Substantial thermoelectric enhancement achieved by manipulating the band structure and dislocations in Ag and La co-doped SnTe. Journal of Advanced Ceramics 10(4):860–870
4. Zheng ZH, Niu JY, Ao DW et al (2021) In-situ growth of high-performance (Ag, Sn) co-doped CoSb3 thermoelectric thin films. Journal of Materials Science Technology 92:178–185
5. Shi XL, Ai X, Zheng QH et al (2020) Enhanced thermoelectric properties of hydrothermally synthesized n-type Se&Lu-codoped Bi2Te3. Journal of Advanced Ceramics 9(4):424–431
6. Fan P, Wei M, Zheng ZH et al (2019) Effects of Ag-doped content on the microstructure and thermoelectric properties of CoSb3 thin films. Thin Solid Films 679:49–54
7. Wei M, Chen TB, Hu JG et al (2020) Effect of organic nano-components on the thermoelectric properties of Sb2Te3 nanocrystal thin film. Scripta Mater 185:105–110
8. He Z, Chen YX, Zheng Z et al (2020) Enhancement of thermoelectric performance of N-type Bi2Te3 based thin films via in situ annealing during magnetron sputtering. Ceram Int 46(9):13365–13371

9. Fan P, Li R, Chen YX et al (2020) High thermoelectric performance achieved in Bi0.4Sb1.6Te3 films with high (00l) orientation via magnetron sputtering. J Eur Ceram Soc 40(12):4016–4021
10. Zheng ZH, Yang D, Zhang PC et al. Enhancement of the thermoelectric properties of Bi2Te3 nanocrystal thin films by rapid annealing. *Materials Letters* 2020
11. Ruan M, Li F, Chen Y et al. Te-free compound Bi2SeS2 as a promising mid-temperature thermoelectric material. *Journal of Alloys and Compounds* 2020
12. Jiang C, Wei P, Ding Y et al. Ultrahigh performance polyvinylpyrrolidone/Ag2Se composite thermoelectric film for flexible energy harvesting. *Nano Energy* 2021
13. Zheng ZH, Yang D, Huang, Xl et al (2020) High-performance zinc antimonide thermoelectric thin films achieved by a layer-by-layer combination reaction approach. J Mater Sci: Mater Electron 31(19):16968–16974
14. Chen YX, Li R, He Z et al (2020) Effects of annealing process on thermoelectric performance for Pb-doped BiCuSeO. J Mater Sci: Mater Electron 31(23):21623–21631
15. Wang Y, Liu WD, Shi XL et al. Enhanced thermoelectric properties of nanostructured n-type Bi2Te3 by suppressing Te vacancy through non-equilibrium fast reaction. *Chemical Engineering Journal* 2020
16. Duan HZ, Li YL, Zhao KP et al (2016) Ultra-Fast Synthesis for Ag2Se and CuAgSe Thermoelectric Materials. Jom 68(10):2659–2665
17. Perez TJA, Caballero CO, Vera LL et al. High Thermoelectric zT in n-Type Silver Selenide films at Room Temperature. *Advanced Energy Materials* 2018
18. Lu Y, Qiu Y, Cai K et al (2020) Ultrahigh power factor and flexible silver selenide-based composite film for thermoelectric devices. Energy Environ Sci 13(4):1240–1249
19. Lu Y, Qiu Y, Cai K et al (2020) Ultrahigh power factor and flexible silver selenide-based composite film for thermoelectric devices: A correction. Energy Environ Sci 13(4):1287–1288
20. Zhou K, Chen J, Zheng R et al (2016) Non-epitaxial pulsed laser deposition of Ag2Se thermoelectric thin films for near-room temperature applications. Ceram Int 42(10):12490–12495
21. Ding Y, Qiu Y, Cai K et al. High performance n-type Ag2Se film on nylon membrane for flexible thermoelectric power generator. *Nat Commun* 2019
22. Gao J, Miao L, Lai H et al. Thermoelectric Flexible Silver Selenide Films: Compositional and Length Optimization. *iScience* 2020, **23**(**1**): 100753
23. Santhosh KMC, Pradeep B (2002) Transport properties of silver selenide thin films from 100 to 300 K. Materials Letters - MATER LETT 56:491–495
24. Gnanadurai P, Soundararajan N, Sooriamoorthi CE (2005) Influence of heating rate on the hysteresis in the phase transition in silver selenide thin films. Vacuum 78(1):33–36
25. Pandiaraman M, Soundararajan N, Vijayan C et al. Spectroscopic studies on silver selenide thin films. *Journal of Ovonic Research* 2010
26. Hussain S, Chae J, Akbar K et al. Fabrication of Robust Hydrogen Evolution Reaction Electrocatalyst Using Ag2Se by Vacuum Evaporation. *Nanomaterials (Basel)* 2019, 9(**10**)

27. Wu Z, Wu J, Li Y et al (2020) Effect of Cu content on electrical properties of evaporated Cu-Se thermoelectric films. Ceram Int 46(13):21617–21622
28. Tang R, Wang Z, Li W et al (2014) Bi2Te3 thin films prepared by co-evaporation for CdTe thin film solar cells. Sol Energy Mater Sol Cells 121:92–98
29. Zhang L, Li Y, Li C et al (2017) Scalable Low-Band-Gap Sb2Se3 Thin-Film Photocathodes for Efficient Visible-Near-Infrared Solar Hydrogen Evolution. ACS Nano 11(12):12753–12763
30. Jindal S, Singh S, Saini GSS et al. Enhanced thermopower in (013)-oriented silver selenide films produced by thermal annealing. *Applied Physics A* 2020
31. Hou S, Liu Y, Yin L et al. High performance wearable thermoelectric generators using Ag2Se films with large carrier mobility. *Nano Energy* 2021
32. Jindal S, Singh S, Saini GSS et al. Low temperature thermoelectric power factors of thermally evaporated Ag2Se thin films. *In 3rd International Conference on Condensed Matter and Applied Physics (Icc-*2019) 2020
33. Lee C, Park YH, Hashimoto H. Effect of nonstoichiometry on the thermoelectric properties of a Ag2Se alloy prepared by a mechanical alloying process. *Journal of Applied Physics* 2007
34. Yang F, Xiong S, Xia Z et al. Two-step synthesis of silver selenide semiconductor with a linear magnetoresistance effect. *Semiconductor Science and Technology* 2012, 27(**12**)
35. Mohanty BC, Kasiviswanathan S (2006) Thermal stability of silver selenide thin films on silicon formed from the solid state reaction of Ag and Se films. Thin Solid Films 515(4):2059–2065
36. Tveryanovich YS, Razumtcev AA, Fazletdinov TR et al (2018) Fabrication of stoichiometric oriented Ag2Se thin film by laser ablation. Thin Solid Films 666:172–176
37. Mogwitz B, Korte C, Janek J et al. Preparation and magnetoresistance of Ag2 + xSe thin films deposited via pulsed laser deposition. *Journal of Applied Physics* 2007, 101(**4**)
38. Milašienė D, Ivanauskas R (2013) Silver selenide modification of polyamide fabric. Open Chemistry 11(12):1976–1980
39. Kreutzbruck MV, Mogwitz B, Gruhl F et al. Magnetoresistance in Ag[sub 2 + δ]Se with high silver excess. *Applied Physics Letters* 2005
40. Mohanty BC, Malar P, Osipowicz T et al (2009) Characterization of silver selenide thin films grown on Cr-covered Si substrates. Surf Interface Anal 41(3):170–178

Figures

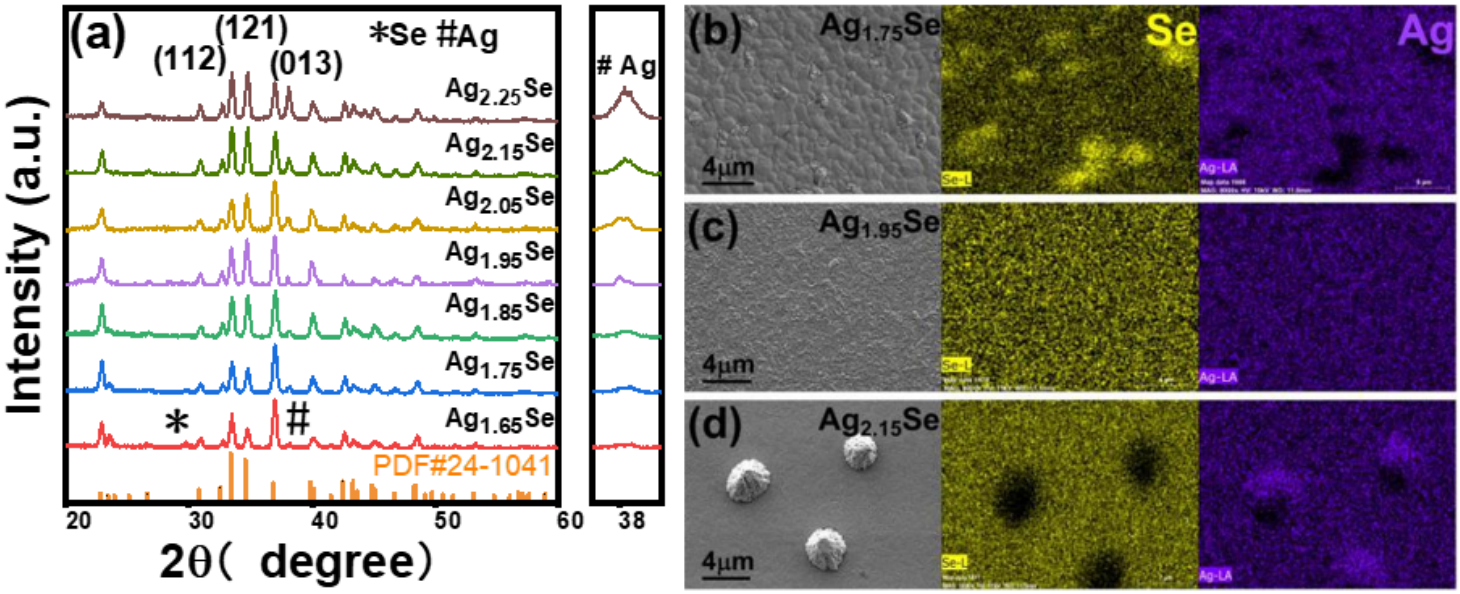

Figure 1

(a) X-ray diffraction patterns of Ag2Se thin films with different nominal ratio of Ag to Se. (b) Surface morphology and elemental mappings of Ag1.75Se, Ag1.95Se and Ag2.15Se thin films

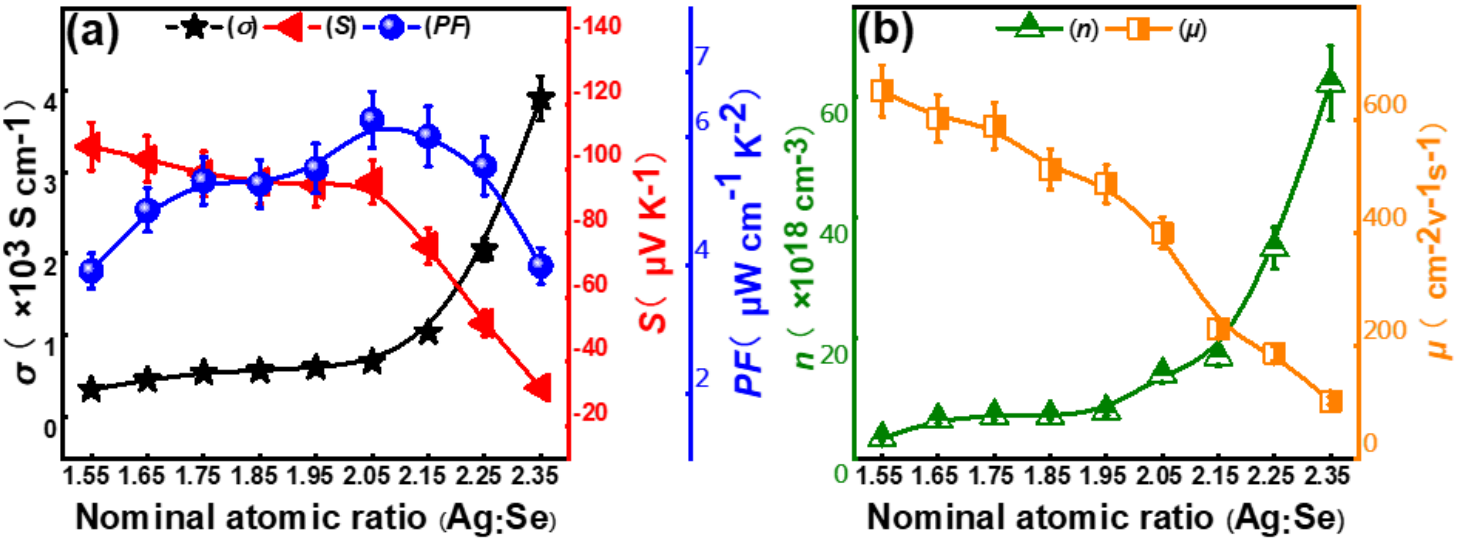

Figure 2

(a) Room-temperature electrical conductivity σ, Seebeck coefficient S and power factor PF; (b) Carrier concentration n and mobility μ of the Ag2Se thin films with different nominal ratio of Ag to Se.

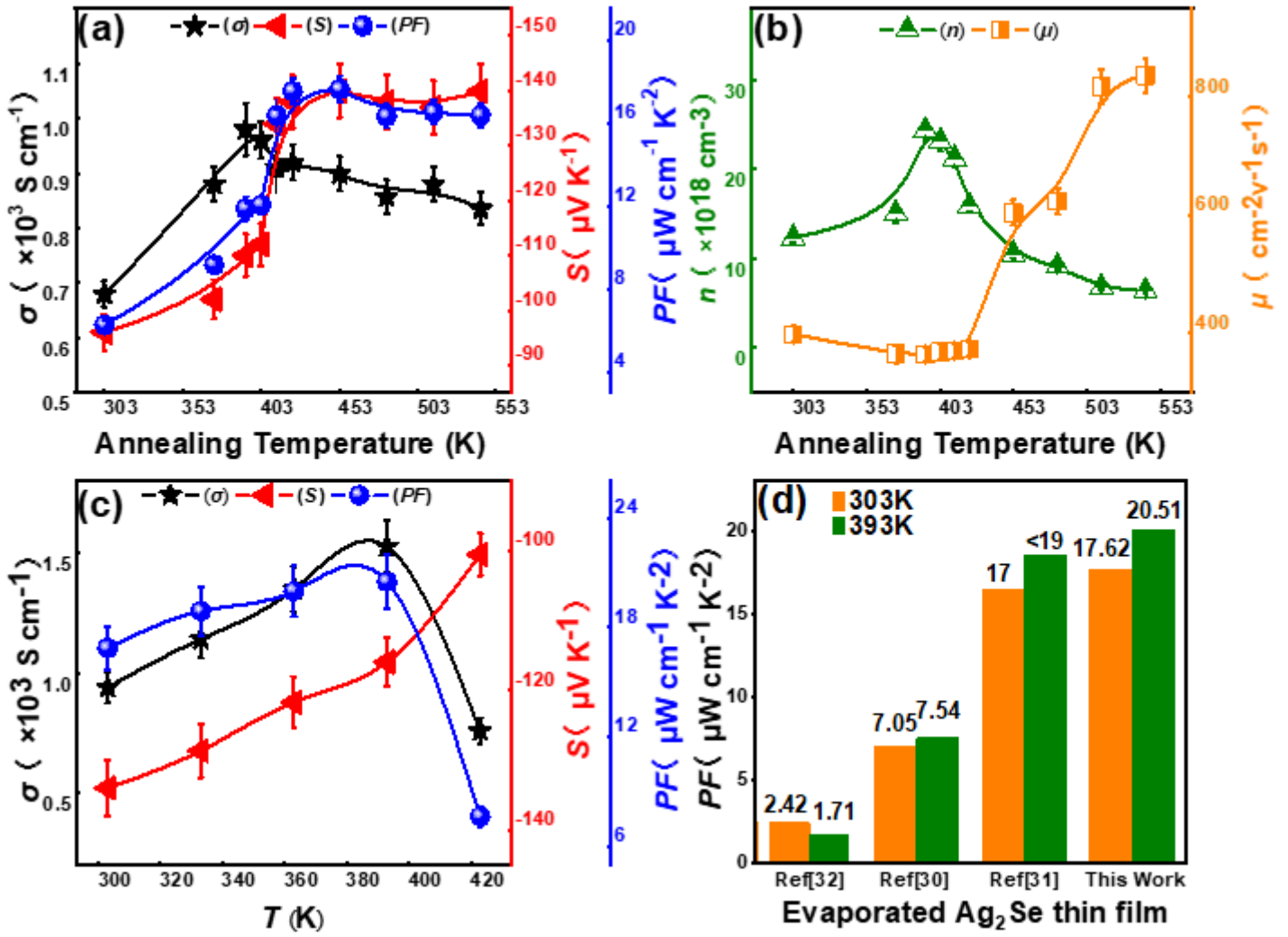

Figure 3

(a) Electrical conductivity σ, Seebeck coefficient S and power factor PF as a function of annealing temperature for Ag2.05Se sample. (b) Carrier concentration n and mobility μ of the annealed samples. (c). Temperature dependence of σ, S and PF of the thin film annealed at 423 K. (d) The comparison of power factor (300 K and 393 K) of Ag2Se thin films prepared by thermal evaporation method [30-32].

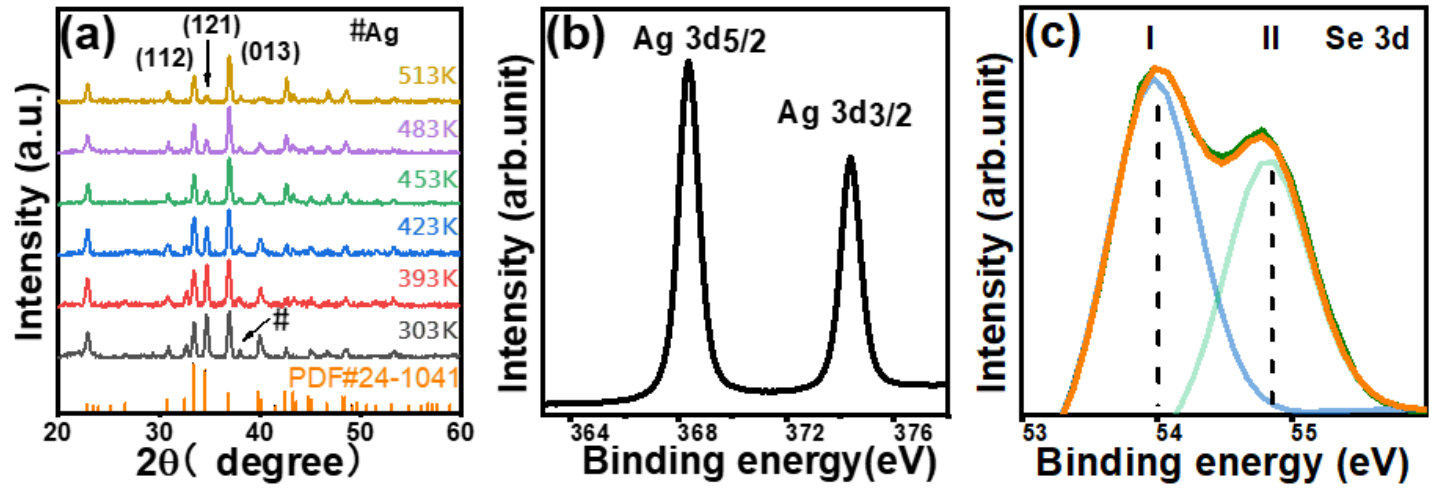

Figure 4

(a) X-ray diffraction patterns of Ag2Se thin films with different annealing temperature. XPS survey scans of Ag2.05Se thin film (b) Ag and (c) Se.

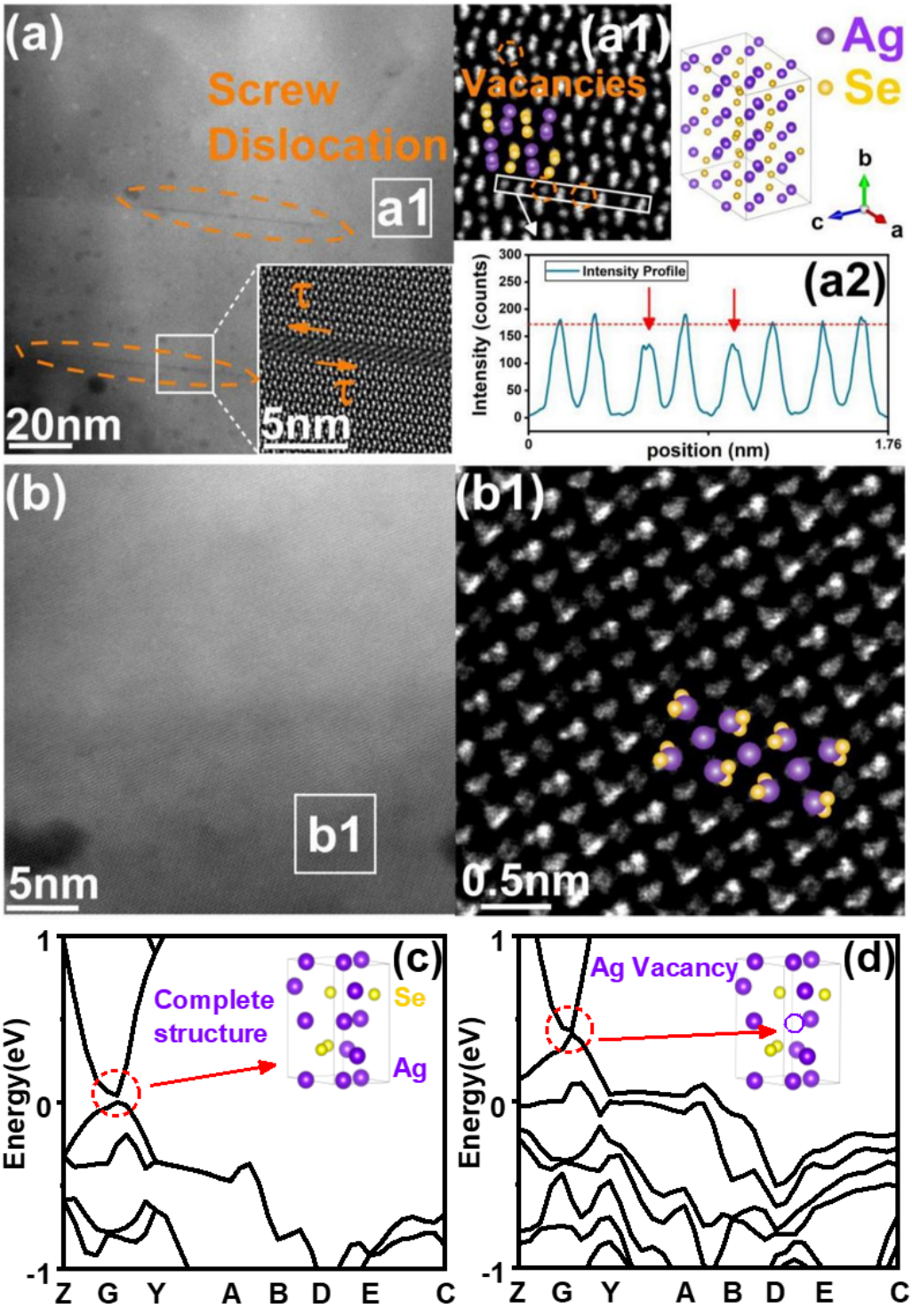

Figure 5

(a) TEM photographs of the Ag2.05Se film before heat treatment, screw dislocation and Ag vacancies (a1) are observed in the lattices; (a2) Intensity line profile of the square root of STEM intensity. (b) Low magnifiation TEM and high resolution TEM images of the Ag2.05Se after annealing at 423 K. (c) Band structure and lattice structure of primary phase of silver selenide. (d) Band structure and lattice structure of silver selenide contain vacancy defects.

Supplementary Files

This is a list of supplementary files associated with this preprint. Click to download.

- supportinginformation0817.docx